

quantum interference device (SQUID) magnetometer between 5 and 300 K and for magnetic fields up to 4 T. The resistivity (ρ) was measured by a standard in-line, four-probe technique and a commercial ac resistance bridge (operating at 16 Hz) at temperatures between 5 and 300 K and at magnetic fields up to 8 T.

10. Data were collected at 298 and 50 K with a Cu(220) monochromator (wavelength $\lambda = 1.5543 \text{ \AA}$) and a Cu(311) monochromator ($\lambda = 1.5396 \text{ \AA}$), respectively, on the 32-detector BT-1 diffractometer at the National Institute of Standards and Technology's research reactor. A figure containing the 50 K data with a fitted profile from Rietveld refinement is available at <http://www.sciencemag.org/science/feature/beyond/#subramanian>. The neutron sample was a pellet weighing 185 mg, which was loaded into a vanadium tube and positioned in the center of the neutron beam. For the 298 K neutron data set, aluminum in the sample mount was incompletely shielded. The resulting aluminum peaks were fit as a second phase with a Le Bail fit [A. Le Bail, H. Duroy, J. L. Fourquet, *Mater. Res. Bull.* **23**, 447 (1988)]. At both temperatures, small peaks from vanadium scattering were also observed and were modeled as an additional phase.
11. A. C. Larson and R. B. Von Dreele, *Rep. LA-UR-86-748* (Los Alamos National Laboratory, Los Alamos, NM, 1986). Refinement statistics for the neutron data at 50 and 298 K are as follows: $\chi^2 = 0.819$ and 0.936 , $R_{wp} = 7.7$ and 3.8% , and $R_{exp} = 6.2$ and 3.2% , for 69 and 65 unique reflections, respectively. The single-crystal XRD refinement with full anisotropic thermal factors, anomalous scattering terms for Ti and Mn, and no absorption correction (19% variation in the azimuthal scan) gave $R_w = 1.3\%$ and $R = 1.6\%$, with 60 unique reflections ($>3\sigma$).
12. M. A. Subramanian *et al.*, *J. Solid State Chem.* **72**, 24 (1988).
13. When we used an anisotropic thermal factor model and fixed the Mn and O^l occupancies at 1, refinement for Ti and O^l site occupancies from x-ray single-crystal refinements resulted in nearly ideal occupancies, giving a composition of $Ti_{2.000(12)}Mn_2O_6^{O^l}_{0.972(17)}$ (numbers in parentheses indicate the error in the last digits). In the neutron refinements, it was not possible to simultaneously vary thermal factors and occupancies; thus, these occupancies were set to unity in the refinements. However, a conservative lower limit on the O^l site occupancy is 0.965 because smaller values result in negative thermal factors. We conclude that there are no Ti or O^l vacancies within the accuracy of the experimental measurements.
14. R. D. Shannon, *Acta Crystallogr. A* **32**, 751 (1976).
15. H. S. Jarrett *et al.*, in *Valence Instabilities and Related Narrow Band Phenomena*, R. D. Parks, Ed. (Plenum, New York, 1977), p. 545; M. A. Subramanian and A. W. Sleight, in *Handbook on the Physics and Chemistry of Rare Earths*, K. A. Gschneider Jr. and L. Eyring, Eds. (Elsevier, Amsterdam, 1993), vol. 10, p. 225.
16. E. O. Wollan and W. C. Koehler [*Phys. Rev.* **100**, 545 (1955)] and Z. Jiráček, S. Krupicka, Z. Simsa, M. Dlouhá, and S. Vratislav [*J. Magn. Magn. Mater.* **53**, 153 (1985)], for example, have reported such magnetic structure determinations for a number of manganese oxide perovskites.
17. G. Shirane, *Acta Crystallogr.* **12**, 282 (1959).
18. We have recently obtained data that substantiate this lack of significant doping through an x-ray absorption near-edge spectroscopy (Mn K edge) study of $Ti_2Mn_2O_7$ (H. D. Rosenfeld and M. A. Subramanian, unpublished material). The Mn K edge of $Ti_2Mn_2O_7$ coincides with the K edges observed for $Mn^{4+}O_2$ and pyrochlore $Er_2Mn_2^{4+}O_7$, both containing only Mn^{4+} . In addition, the K edge of $Ti_2Mn_2O_7$ also shows appropriate shifts from the K edges observed for $Mn^{3+}O_3$ and CMR perovskite $La_{0.3}^{3+}Sr_{0.3}^{2+}Mn^{3.3+}O_3$.
19. P. Shiffer, A. P. Ramirez, W. Bao, S.-W. Cheong, *Phys. Rev. Lett.* **75**, 3336 (1995).
20. J. B. Goodenough, *Magnetism and the Chemical Bond* (Krieger, New York, 1976), p. 184.
21. M. E. Fisher and J. S. Langer, *Phys. Rev. Lett.* **20**, 665 (1968).

22. We thank Q. Z. Huang, M. K. Crawford, J. E. Greedan, A. C. Larson, and C. Broholm for useful discussions on the magnetic refinements, R. L. Harlow for help in the single-crystal work, and T. G. Calvarese and M. L. Plummer for help in the high-pressure synthesis. The work at Lawrence Liver-

more was done under the auspices of the U.S. Department of Energy under contract W-7405-ENG-48. A.W.S. thanks NSF for research grant DMR-9308530.

18 March 1996; accepted 29 May 1996

Direct, Nondestructive Observation of a Bose Condensate

M. R. Andrews, M.-O. Mewes, N. J. van Druten, D. S. Durfee, D. M. Kurn, W. Ketterle

The spatial observation of a Bose condensate is reported. Dispersive light scattering was used to observe the separation between the condensed and normal components of the Bose gas inside a magnetic trap. This technique is nondestructive, and about a hundred images of the same condensate can be taken. The width of the angular distribution of scattered light increased suddenly at the phase transition.

Bose-Einstein condensation (BEC) is characterized by a macroscopic population of particles in the quantum-mechanical ground state below a critical temperature. It is the origin of macroscopic quantum phenomena such as superfluidity in liquid helium (1). For a homogeneous sample, BEC is sometimes called "condensation in momentum space" (2) because it does not lead to a spatial separation between the condensate and the normal component. However, in any inhomogeneous potential—for example, in atom traps or even in Earth's gravitational field—the condensate and the normal fraction of a Bose gas are spatially separated (2, 3). So far, BEC has only been seen in momentum space: the condensate fraction of liquid helium was determined by neutron scattering (4), the condensation of excitons was deduced from the observed energy distribution of the excitonic particles (5), and BEC in dilute atomic gases was detected by observation of the velocity distribution of freely expanding Bose condensates (6, 7). We report the direct and nondestructive observation of the spatially localized condensate in a gas of magnetically trapped sodium atoms.

Bose condensates of dilute atomic gases are a new form of quantum matter. The pioneering work toward BEC in atomic gases was done with spin-polarized hydrogen with the use of magnetic trapping and evaporative cooling (8). In work at JILA (9) and the Massachusetts Institute of Technology (10), these techniques were successfully combined with laser cooling (11), which resulted in the observation of BEC in rubidium in June (6) and in sodium in September of 1995 (7). Lithium has also been

cooled to the quantum degenerate regime (12). Since these developments, there has been a flurry of both theoretical and experimental activity (13).

In atom traps, the condensation phenomenon results in the formation of a dense core of atoms in the ground state of the system surrounded by the normal component—analogue to droplet formation in a saturated vapor. Our earlier attempts to observe the Bose condensate directly by absorption imaging failed because of the high optical density of the atom cloud near the critical temperature. For typical parameters of our experiment, the peak optical density D_0 for resonant light was about 300, corresponding to a transmission coefficient of e^{-300} . Thus, the probe light was completely absorbed, even in the wings of the spatial distribution, preventing direct imaging of the condensate. Detuning of the light, which reduced the absorption, revealed major image distortions caused by dispersive effects: the condensate acted as a lens and strongly deflected the light. However, by using the so-called "dark-ground" imaging technique (14), we were able to use the dispersively scattered light to clearly image the condensate.

Dispersive imaging has significant advantages over absorption methods for the imaging of small and dense clouds ($D_0 \gg 1$). To obtain a good absorption signal, one would like to detune the probe light until the off-resonant optical density D is close to unity; D is given by $D = D_0/\Delta^2$, where the detuning Δ from the resonant frequency ω_0 is $\Delta = 2(\omega - \omega_0)/\Gamma$, with Γ being the natural linewidth. The maximum phase shift δ of the transmitted wave is $\delta = D_0/2\Delta$, and thus for $D \sim 1$, the phase shift is $\delta \sim \sqrt{D_0}/2$. Such a large phase shift is caused by lenslike refraction, which bends

Department of Physics and Research Laboratory of Electronics, Massachusetts Institute of Technology, Cambridge, MA 02139, USA.

the incident probe light beyond the cloud's diffractive scattering angle. If the spatial resolution of the imaging system is well matched to the small size of the cloud, this refracted light is not collected by the optics; therefore, absorption images of small and dense clouds are unavoidably degraded. In order to use the imaging system at its nominal resolution, detunings on the order of D_0 are necessary, where absorption signals are negligible, but dispersive phase shifts are close to unity. The signal in dispersive imaging depends on this phase shift, yielding a viable method for probing small and dense clouds.

This argument can be quantified by considering the small, dense cloud to be a lens. A sphere of radius R and index of refraction n acts as a lens having focal length f with $1/f = 2(n - 1)/R$ (14). The phase shift δ of light at wavelength λ passing through the center of the lens is $\delta = 4\pi R(n - 1)/\lambda$, yielding $f = 2\pi R^2/\delta\lambda$, and the maximum deflection angle θ for the light is approximately $\theta \approx R/f = (2\delta/\pi) \times (\lambda/4R)$. If $\delta > \pi/2$, light will be deflected as a result of refraction at an angle that exceeds the scattering angle $\lambda/4R$ due to diffraction. As long as the imaging system collects and images the refracted light, quantitative absorption imaging is possible. However, the radius R of the smallest object that can be resolved is usually determined by the collection angle α of the optics to be $R = \lambda/2\alpha$. Additional refraction by the object will scatter light out of the optical system and impede absorption measurements. Therefore, dispersive refraction limits the use of absorption imaging to objects $\approx 2\delta/\pi$ times as large as the diffraction-limited value of $R = \lambda/2\alpha$.

Dispersive scattering is the coherent forward scattering of light. In a homogeneous medium, the scattered light interferes constructively only in the direction collinear with the incident light. Interference with the transmitted beam results in a phase shift and is described by the usual theory for the index of refraction (14). In contrast, for an inhomogeneous medium of extension $2R$, such as a trapped cloud of atoms, the coherently scattered light interferes constructively in an angular region $\lambda/2R$. The scattered light can be separated from the incident light in the Fourier transform plane of the imaging system. The incident beam comes to a focus there and can be blocked by a small opaque object. This "dark-ground" method is common in microscopy and is related to Schlieren and phase contrast methods (14). In all of these methods, the image is modified in the Fourier plane, enhancing the contrast or the sensitivity for phase objects.

In our experiment, sodium atoms were cooled down to BEC by a combination of

laser cooling, magneto-optic trapping, magnetic trapping, and evaporative cooling. The atom cloud was confined in a magnetic trap that uses cloverleaf coils to generate the inhomogeneous magnetic field (15). Near the bottom of the trap, the potential was harmonic and axially symmetric, with independently adjustable axial and radial confinement. We controlled the evaporative cooling by continuously reducing the frequency of rf (radio frequency) radiation. The rf field induces spin flips at a specific value of the magnetic field where the condition for electron spin resonance is met. Because the spin flips reverse the sign of the magnetic force on the atoms, the spin-flipped atoms are ejected from the trap (16); in this way, the rf frequency determines an effective trap depth. The escape of the hottest atoms from the trap, in combination with rethermalization of the remaining atoms through elastic collisions, cools the sample (evaporative cooling) to a temperature that is about 10% of the effective trap depth.

Typically, we reached the BEC phase transition with 1.5×10^7 atoms in the $F = 1$, $m_F = -1$ hyperfine state at a temperature of $1.5 \mu\text{K}$ and a number density of 10^{14} cm^{-3} . Further cooling resulted in the formation of a nearly pure condensate with 5×10^6 atoms (15). Temperature and number were determined by a time-of-flight technique in which the trap was suddenly switched off and the cloud expanded ballistically. The expanding cloud became dilute, and quantitative absorption images could be taken. The temperature was derived from the root mean square (rms) velocity of the cloud's normal component, and the number was obtained from the total light absorption.

To image the cloud with the use of dispersive light scattering, we detuned the probe light frequency by 1.71 GHz ($\Delta = -342$) to the red of the $F = 1$ to $F = 2$ optical transition (17). The cloud was imaged with a CCD (charge-coupled device) sensor using a lens system with a resolution of $5 \mu\text{m}$. A thin wire (0.2 or 1.0 mm) in the Fourier plane of the lens system blocked the transmitted unscattered light (dark-ground imaging). We obtained the images by exposing the trapped atoms to weak probe light for 0.5 s after the loading and cooling procedure. For each image, a new cloud was loaded and cooled to a progressively lower temperature. In this way, we were able to monitor the growth of the condensate fraction within the saturated Bose gas (Fig. 1). The number of atoms in the normal component saturates at $1.202(k_B T/\hbar\bar{\omega})^3$ (18), where k_B is Boltzmann's constant, T is the temperature, \hbar is Planck's constant divided by 2π , and $\bar{\omega}$ is the geometric mean of the

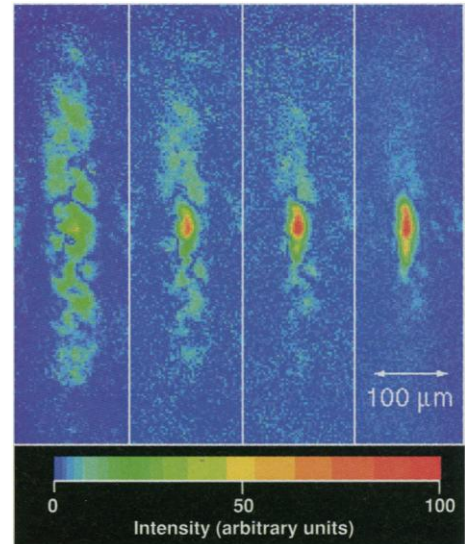


Fig. 1. Direct observation of BEC of magnetically trapped atoms by dispersive light scattering. The probe laser beam propagates along a radial direction of the trap. The clouds have condensate fractions that increase from close to 0% (left) to almost 100% (right). This series was taken at axial and radial field curvatures of 0.1 and 3 kG/cm^2 , respectively, resulting in an aspect ratio of the trapped cloud of about 6. The signal for the normal component is rather weak and interferes with the speckle pattern of stray laser light, giving it a patchy appearance.

three harmonic trapping frequencies. Lowering the temperature forces the atoms that exceed this number to condense, similar to droplet formation in a saturated vapor. We measured the effective area of the cloud as observed in dark-ground imaging versus final rf frequency. The sudden decrease in area at the onset of BEC (at an rf frequency of 1200 kHz) (Fig. 2) is a sensitive indicator for the phase transition.

Dispersive imaging is a nondestructive technique and allows many pictures of the same condensate to be taken. Absorption imaging relies on incoherent large-angle (Rayleigh and Raman) scattering. Each scattering event heats an atom by an aver-

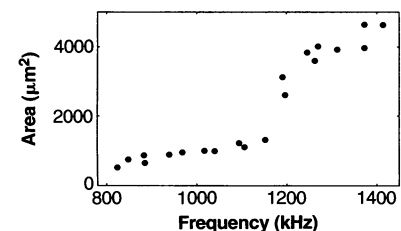


Fig. 2. Effective area of the atom cloud in dark-ground imaging versus final rf frequency, which is approximately linearly related to temperature. The effective area is defined as the total amount of scattered light divided by the peak scattered intensity. The sudden decrease in the effective area indicates the BEC phase transition.

age energy of $(\hbar k)^2/m = 2.3 \mu\text{K} \times k_B$, which is twice the single-photon recoil energy ($\hbar k$ denotes the photon momentum, and m is the atomic mass). In dispersive scattering, the photons are elastically scattered by only a small angle $\lambda/4R$, which was typically 0.02 rad in our experiment. The recoil energy of this process is about 0.5 nK, 1/2000th of the single-photon recoil energy. Furthermore, when the probe pulse duration is much longer than the oscillation period in the trap, the momentum transfer to an individual atom averages out; hence, no heating is associated with the coherent forward scattering of light. This suppression of heating can be regarded as a Mössbauer effect, where the momentum is absorbed by the trap and not by individual atoms. An alternative explanation uses the concept of light forces. For light detuned to the red of the atomic resonance, the incident plane wave is focused (because the index of refraction is greater than one). As a consequence, the light exerts an outward force on the atoms through the stimulated light force (or the optical dipole force). If this force is switched on and off adiabatically, there is no heating.

To test the nondestructive nature of dispersive imaging, we imaged the same condensate twice with a delay time of 1 s: There was no observable reduction in the signal (Fig. 3A). When the incident pulse energy of the probe light was increased to $2 \mu\text{J}/\text{cm}^2$, the signal in the second image deteriorated. At this energy, 5×10^6 scattered photons were detected, which is sufficient to allow 100 consecutive images of the same condensate to be taken. We estimate that under these conditions, the probability for off-resonant absorption was about 4%, implying an energy transfer of around 100 nK

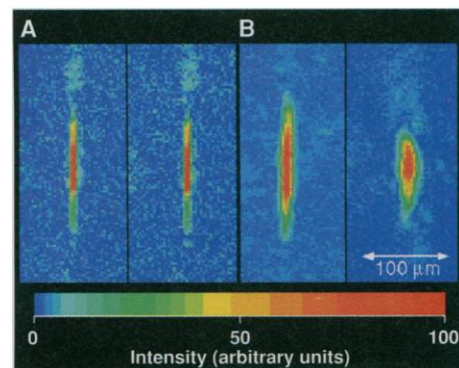


Fig. 3. Demonstration of nondestructive imaging. **(A)** Images of the same condensate taken 1 s apart. The axial and radial field curvature were 0.1 and 30 kG/cm², respectively, resulting in an aspect ratio of the trapped cloud of about 20. **(B)** Dynamics of a single condensate. The two pictures were taken 6 s apart during radial decompression of the cloud. The final radial field curvature (right) was 3 kG/cm².

per atom in the cloud. It is therefore likely that the limit to the probe pulse energy was set by residual absorption and can be further reduced with the use of larger probe-light detunings.

Short probe pulses would provide good temporal resolution at the expense of suppressing the Mössbauer effect. For probe durations shorter than the oscillation time, the atoms should behave as free particles and receive recoil kicks of 0.5 nK per forward-scattered photon. For our conditions, this energy is negligible compared with the heating from residual absorption. In agreement with this calculation, no difference in the maximum nondestructive probe pulse energy was observed when the pulse duration was varied between 2 and 200 ms. The shortest exposure time was comparable to the radial oscillation period (3 ms). Shorter pulses with the same energy could not be applied because of limitations in probe power but are possible and would give even better temporal resolution.

The ability to take several nondestructive images is useful for the study of the dynamics of a single condensate, such as its formation, decay, and response to external forces (Fig. 3B). If studies are done destructively, each time step is taken with a new sample, and shot-to-shot fluctuations may be limiting.

The angular distribution of the scattered light is anisotropic because of the elongated shape of the cloud. For a dilute sample, the angular distribution is determined by the Fourier transform of the spatial distribution. At low density, the scattering is weak and covers an angle of about $\lambda/4R$. Increasing the density increases only the intensity of the scattered light. However, when the phase shift across the sample approaches $\pi/2$, the cloud behaves as a lens and refracts

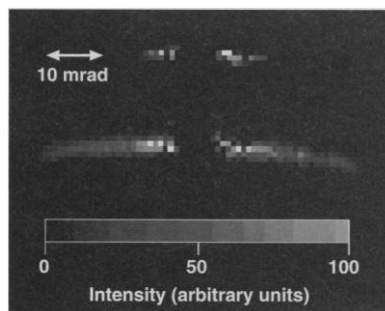


Fig. 4. Angular distribution of the scattered light. The trapping field curvatures are the same as in Fig. 3A. The figure shows the intensity of the scattered light in the Fourier plane of the imaging system, that is, the intensity as a function of the radial and axial scattering angles. The upper image is for a cloud just above BEC, and the lower one is for an almost pure condensate. The central parts of the images are obscured by a 1.0-mm-diameter wire blocking the undeflected probe beam.

the incident light with a mean angular deflection larger than $\lambda/4R$ (as estimated above). Further increase of the density will increase the deflection angle.

At a detuning of 1.71 GHz and an estimated resonant optical density of 300, the maximum phase shift is about 0.5, which means that we are still in the diffractive regime but close to the transition where refraction becomes important. Between 10 and 100% of the incident probe light intensity was deflected by the condensate.

By focusing the camera onto the Fourier plane of the first imaging lens, we were able to directly record the angular distribution of scattered light. The BEC phase transition was accompanied by a sudden increase of the scattering angle. The rms scattering angle of the thermal cloud, ≈ 7 mrad, is the diffraction angle of a cloud with radial diameter $20 \mu\text{m}$, in agreement with the size of a $1.5\text{-}\mu\text{K}$ cloud in the magnetic trapping potential (Fig. 4). The angular scattering pattern of the condensate has an rms width of ≈ 20 mrad, in agreement with the size and shape of the condensate as calculated by the nonlinear Schrödinger equation and the Thomas-Fermi approximation (19).

The results presented here demonstrate that dispersive light scattering is an important method for study of BEC. Although we have emphasized qualitative aspects in the present study, quantitative measurements are possible because the signal in dispersive imaging depends only on the phase shift δ ; δ is an absolute measure of the line-of-sight integrated atomic density. For small phase shifts, which are obtained at large detunings, the fraction of scattered light in dark-ground imaging is δ^2 . A signal linear in δ can be obtained by implementing the phase contrast method.

This work is the starting point for a systematic study of the optical properties of a Bose condensate (20). Additional measurements at 100-MHz detuning showed several fringes in dark-ground images as a result of phase shifts $\delta > 2\pi$. We are currently setting up an independent dye laser to characterize the optical properties of the condensate starting from large detunings. It has been predicted that the linewidth of a Bose condensate shows superradiant broadening (21). On the other hand, the dispersive signal at far detuning is independent of the linewidth and therefore particularly suited for quantitative measurements. Quantum-statistical effects on the index of refraction have been calculated (22) but are only noticeable near the phase transition and vanish at $T = 0$.

We have presented dispersive light scattering as a nondestructive method. Strictly speaking, however, quantum mechanics does not allow nonperturbative measurements. Although dispersive scattering does

not heat up the cloud and destroy the condensate, it will change its phase as a result of frequency shifts by the ac Stark effect. This still allows a nonperturbative measurement of the number of condensed atoms, which is the variable complementary to the phase (so-called quantum nondemolition measurement), and would be the inverse situation compared to related measurements in microwave cavities where the photon number can be determined from the phase shift of Rydberg atoms passing through the cavity (23).

REFERENCES AND NOTES

1. A. Griffin, D. W. Snoke, S. Stringari, Eds., *Bose-Einstein Condensation* (Cambridge Univ. Press, Cambridge, 1995).
2. K. Huang, *Statistical Mechanics* (Wiley, New York, ed. 2, 1987).
3. W. E. Lamb Jr. and A. Nordsieck, *Phys. Rev.* **59**, 677 (1941).
4. P. E. Sokol, in (1), pp. 51–85.
5. J. L. Lin and J. P. Wolfe, *Phys. Rev. Lett.* **71**, 1222 (1993).
6. M. H. Anderson, J. R. Ensher, M. R. Matthews, C. E. Wieman, E. A. Cornell, *Science* **269**, 198 (1995).
7. K. B. Davis et al., *Phys. Rev. Lett.* **75**, 3969 (1995).
8. T. J. Greytak, in (1), pp. 131–159.
9. W. Petrich, M. H. Anderson, J. R. Ensher, E. A. Cornell, *Phys. Rev. Lett.* **74**, 3352 (1995).
10. K. B. Davis et al., *ibid.*, p. 5202.
11. E. Arimondo, W. D. Phillips, F. Strumia, Eds., *Proceedings of the International School of Physics "Erice Fermi," Course CXVIII* (North-Holland, Amsterdam, 1992).
12. C. C. Bradley, C. A. Sackett, J. J. Tollett, R. G. Hulet, *Phys. Rev. Lett.* **75**, 1687 (1995).
13. Book of abstracts, *Workshop on Collective Effects in Ultracold Atomic Gases*, Les Houches, France, 1–5 April 1996.
14. E. Hecht, *Optics* (Addison-Wesley, Reading, MA, ed. 2, 1989).
15. M.-O. Mewes et al., *Phys. Rev. Lett.*, in press.
16. D. E. Pritchard, K. Helmerson, A. G. Martin, in *Atomic Physics 11*, S. Haroche, J. C. Gay, G. Grynberg, Eds. (World Scientific, Singapore, 1989), pp. 179–197; W. Ketterle and N. J. van Druten, in *Advances in Atomic, Molecular and Optical Physics*, B. Bederson and H. Walther, Eds. (Academic Press, San Diego, in press), vol. 37.
17. It was a coincidence that the ideal detuning for this work was close to the 1.77 GHz ground-state hyperfine splitting in sodium.
18. S. R. de Groot, G. J. Hooyma, C. A. ten Seldam, *Proc. R. Soc. London Ser. A* **203**, 266 (1950).
19. G. Baym and C. J. Pethick, *Phys. Rev. Lett.* **76**, 6 (1996).
20. L. You, M. Lewenstein, R. J. Glauber, J. Cooper, *Phys. Rev. A* **53**, 329 (1996).
21. J. Javanainen, *Phys. Rev. Lett.* **72**, 2375 (1994).
22. O. Morice, Y. Castin, J. Dalibard, *Phys. Rev. A* **51**, 3896 (1995).
23. M. Brune et al., *Phys. Rev. Lett.* **65**, 976 (1990).
24. We are grateful to D. Pritchard for valuable comments on the manuscript and thankfully acknowledge C. Townsend for assistance in the final stages of the experiment. This work was supported by the Office of Naval Research, NSF, Joint Services Electronics Program, and the Sloan Foundation. M.-O.M. and D.M.K. acknowledge financial support from Studienstiftung des Deutschen Volkes and an NSF Graduate Research Fellowship, respectively, and N.J.v.D., from Nederlandse Organisatie voor Wetenschappelijk Onderzoek (NWO) and Netherlands America Commission for Education Exchange (Fulbright fellowship).

29 May 1996; accepted 11 June 1996

Homogeneous Linewidths in the Optical Spectrum of a Single Gallium Arsenide Quantum Dot

D. Gammon,* E. S. Snow, B. V. Shanabrook, D. S. Katzer, D. Park

The homogeneous linewidths in the photoluminescence excitation spectrum of a single, naturally formed gallium arsenide (GaAs) quantum dot have been measured with high spatial and spectral resolution. The energies and linewidths of the homogeneous spectrum provide a new perspective on the dephasing dynamics of the exciton in a quantum-confined, solid-state system. The origins of the linewidths are discussed in terms of the dynamics of the exciton in zero dimensions, in particular, in terms of lifetime broadening through the emission or absorption of phonons and photons.

Excitons are the quanta of excitation in semiconductors that are composed of an electron excited across the band gap bound to the hole left behind. Localization of the exciton in all three dimensions changes the density of states from a continuous band structure to one that is “atomic-like” and strongly modifies the optical spectrum. Large variations in the magnitude of localization lead to variations in the energies of the different excitons and consequently to inhomogeneous broadening of the spectral features. However, the rate at which a given exciton is scattered is greatly reduced by localization, which dramatically decreases the homogeneous linewidth (1, 2). This effect was first measured in GaAs-Al_xGa_{1-x}As quantum well structures by Hegarty et al. (3) and subsequently by many other groups, although only with the rather indirect methods of nonlinear spectroscopy (1, 4) and light scattering (3, 5, 6) on large inhomogeneous ensembles. We discuss here a direct measurement of the homogeneous linewidth of a single localized exciton.

In narrow quantum wells, localization occurs in one of the dimensions through the quantum-well potential and in the other two dimensions through random variations in the quantum-well width arising from monolayer fluctuations in the position of the interface (schematic in Fig. 1). In some cases, the localized excitons in quantum wells can be treated as a dilute but weakly bound system of “zero-dimensional” (0D) quantum dots (Qdots). Local spectroscopic techniques, such as near-field optical microscopy, can be used to probe an individual Qdot (7–10) and to measure its excited states (9, 10). We can measure directly the homogeneous lin-

ewidth because, by looking at a single Qdot, all inhomogeneous broadening is removed. This allows us to measure the homogeneous linewidth of a localized exciton along with its excited-state spectrum. We can simultaneously obtain a direct measure of the homogeneous linewidths of the exciton ground and excited states and determine the size of the Qdot potential as parameterized by the energy separations of the quantized states. We compare the measured Qdot homogeneous linewidths with those expected if the 0D exciton dynamics (2, 11–13) are dominant-

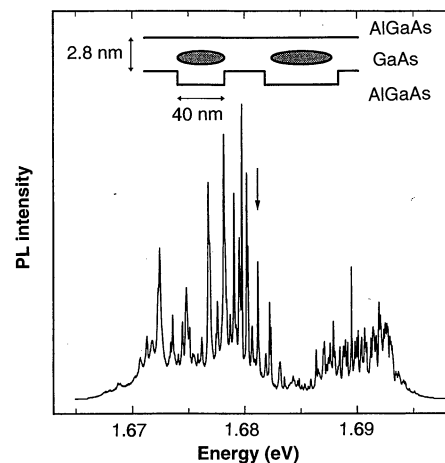


Fig. 1. Nonresonant (laser energy, 2.4 eV) PL measured through an aperture 1.5 μm in diameter. The sharp lines arise from the Qdot potentials discussed in the text. The clustering of the sharp lines into two broad features centered at 1.677 and 1.690 eV arises from fluctuations of one monolayer (0.3 nm) in the quantum-well width, whereas the distribution within the broad peaks arises from fluctuations in the lateral sizes of the Qdots. The arrow points to the Qdot line that is discussed in detail here. The inset shows schematically (not to scale) the monolayer fluctuations in the quantum-well interfaces that lead to the localization of the excitons (ovals) into Qdot potentials.

Naval Research Laboratory, Washington, DC 20375, USA.

*To whom correspondence should be addressed. E-mail: gammon@bloch.nrl.navy.mil